REMOTE SENS. ENVIRON. 34:55–70 (1990)

Comparative Analysis of Landsat-5 TM and SPOT HRV-1 Data for Use in Multiple Sensor Approaches

*Joachim Hill and Dorothea Aifadopoulou**

Institute for Remote Sensing Applications, Laboratory for Image Processing, Commission of the European Communities, Joint Research Center, Ispra, Italy

In view of multiple sensor approaches in remote sensing, we have analyzed the geometric and, in particular, radiometric accuracy of multispectral SPOT HRV (high resolution visible) data in comparison to Landsat-5 Thematic Mapper images. We used concurrent system corrected TM and SPOT images which were recorded almost simultaneously over the southern Ardèche region (France). The TM and SPOT scenes were registered to map projection with subpixel accuracy, but the mountainous character of the study region required the use of digital elevation data for the compensation of relief induced distortions. Our radiometric comparison of the TM and SPOT sensors involved an analysis of the calibration accuracy and a comparison of spectral greenness and brightness features which can be obtained from the two systems. The calibration assessments were primarily based upon the apparent reflectances of bare soil reference targets, and the in-flight calibration of both sensor systems was found in accordance with the respective specifications. For the comparative analysis of spectral features we used an extended set of targets, representing a wide range of vegetated and nonvegetated cover types. In order to directly relate the image-based relations to those obtained from field radiometry data, we had to correct the TM and SPOT data for atmospheric absorption, scattering and pixel adjacency effects. Both systems provide slightly different brightness and greenness information (Tasseled Cap equivalent brightness and greenness, normalized difference vegetation index). But these indices appear to be linearly related, and the respective transfer functions permit mutual data adjustments. Therefore, a wide range of applications in agricultural monitoring and vegetation observation can be approached by using multiple sensor data sets which involve TM and SPOT imagery.

INTRODUCTION

The use of multitemporal data sets increases the precision in classification and mapping of ground cover types from high resolution satellite imagery,

Address correspondence to Joachim Hill, Inst. for Remote Sens. Appl., Joint Res. Ctr., Ispra Establishment, I-21020 Ispra (Varese), Italy.

*Mrs. Aifadopoulou is a grantholder of the Commission of the European Communities, Directorate—General of the Joint Research Centre.

Received 11 January 1990; revised 7 September 1990.

0034-4257/90/$3.50

655 Avenue of the Americas, New York, NY 10010

Table 1. Spectral Characteristics of the Landsat-5 TM and the SPOT Systems

Spectral Bands	*Center Wavelength (μm)*	*Bandwidth (μm)*	*Spectral Solar Irradiance ($mW/cm^2/\mu m$)*	*Center Wavelength (μm)*	*Bandwidth (μm)*	*Spectral Solar Irradiance ($mW/cm^2/\mu m$)*
TM1	0.486	0.066	195.70			
XS1				0.544	0.082	187.48
TM2	0.570	0.081	182.90			
XS2				0.638	0.045	164.89
TM3	0.660	0.067	155.70			
XS3				0.816	0.090	110.14
TM4	0.840	0.128	104.70			
TM5	1.676	0.216	21.93			
TM7	2.223	0.252	7.45			

Solar irradiance data from Markham and Barker (1987) and Price (1988).

and it is also felt that a suitable time series may provide a potential tool for monitoring spatial and temporal variations of the terrestrial environment, for change detection and environmental modeling. But many regions in the world are frequently covered by clouds which restrict the data acquisition from optical satellites. The joint use of data from different operational satellite sensors such as the Landsat Thematic Mappers and the SPOT HRVs may provide a solution to partially overcome the acquisition problems, but the multiplicity of data sources does also complicate operational procedures for the data analysis. Since quantitative comparisons are mandatory for monitoring the earth's reflectivity, multiple sensor approaches equally require radiometrically calibrated images and a good comprehension of the spectral features (i.e., greenness and brightness indices) that can be computed with the corresponding spectral bands.

Landsat-5 Thematic Mapper data have a spatial resolution of 30 m with six reflective bands, excluding the thermal band, and the SPOT HRV multispectral data have a 20 m resolution with three spectral bands (Table 1). It is known that, due to TM Bands 1, 7, and, especially, 5, the Landsat data contain spectral information which is not present in the multispectral SPOT data (Bernier et al., 1988; Chavez and Bowell, 1988). But location and bandwidth of the spectral channels in the visible and near-infrared are similar, and appear well suited for the use in multiple sensor approaches. We have therefore analyzed the geometric and radiometric accuracy of Landsat-5 TM and SPOT HRV-1 data, and assessed the relation between corresponding spectral features that can be obtained from both sensors (normalized difference vegetation index, Tasseled Cap greenness and brightness).

Figure 1. Location of the study region.

DATA SETS

We have used TM and SPOT scenes which were almost simultaneously acquired on the same day (29 September 1986) over a study site of the Joint Research Centre (JRC) in the French Département Ardèche (Fig. 1). It is located about 40 km south of the city of Lyon, and extends from the Rhône valley towards the eastern "Massif Central" (Hill and Mégier, 1988). The TM image was acquired as system corrected CCT, and the SPOT scene is a level 1B product.

Table 2. Thematic Mapper and SPOT Scene Characteristics

WRS frames	197/29	47/260&261
Acquisition date	29 Sep. 1986	
Acquisition time	9.49 GMT	10.47 GMT
Scene location	44.6°	44.2°N
	3.72°E	3.85°E
Sun elevation	37.42°	42.20°
Sun azimuth	145.92	163.95°
Instr. tilt	—	R2.4°

The scenes were recorded with a time difference of 1 h only (Table 2). This introduced minor differences of the illumination geometry, but there are indications that the atmospheric conditions did not change significantly. The observation geometry for both data sets comprises only view angles between $-4°$ to $5°$ so that nadir viewing could be assumed for the radiometric analysis. The data set thus provides an almost unique opportunity for a thorough analysis of the radiometric in-flight performance of both systems in 1986.

THE GEOMETRIC REGISTRATION OF THE DATA

The first step in generating multiple sensor data sets is the geometric registration of the images to a common map grid. When merging higher resolution data with lower resolution images, it is usually attempted to use the high resolution image for respective enhancements of the lower resolution data (Haydn et al., 1982; Cliche et al., 1985). We decided to resample both images to a common pixel size of 30 m×30 m in order to minimize radiometric distortions of the geocoded data set, especially the lower resolution data.

It is known that system corrected TM data and SPOT level 1B products are of exceptionally good geometric quality which, over level terrain, allows geodetic rectifications to subpixel precision by means of first-order polynomials (Welch et al., 1985; Welch and Ehlers, 1986). But for high resolution satellite imagery such scene distortions have become important that are due to local variations in terrain altitude (Marvin et al., 1987). The resulting horizontal dislocation of ground features (relief displacement) is known to cause misregistration of multitemporal overlays, especially in high relief areas or when images with different observation geometry are involved.

Since system corrected TM and SPOT level 1B products are already corrected for internal scan distortions (i.e., nonlinearity of mirror motion, earth curvature effects, panoramic distortion, scan skew, and sensor attitude variations), both images form geometrically a series of near-orthogonal projections in along-track direction and, across-track, a series of parallel perspective projections (Kohl and Hill, 1988). The elimination of relief displacement effects can therefore be limited to a simple correction of the respective pixel position within each scan line according to

$$P_y' = P_y \pm h \tan \theta, \tag{1}$$

where P_y' denotes the corrected y-coordinate and P_y is the original position of the pixel within the image line; h is the terrain elevation at the respective map position, and θ gives the observation angle at the image pixel which, in the case of SPOT, comprises also the instrument tilt angle ω. The sign of the offset depends on the pixel position relative to the line nadir (Kohl and Hill, 1988).

This correction must first be applied to the image coordinates of the ground control points (GCPs) in order to compute a mapping function which is not affected by terrain induced image distortions. The geometric rectification of the TM and SPOT scenes then combines an affine transformation and the local correction of terrain dependant pixel displacements, in which the terrain altitude at each geocoded pixel position is obtained from digital elevation data (Kohl and Hill, 1988).

The evaluation of the registration accuracy yielded root-mean-square error (RMSE) values of ±14.8 m for the Landsat-5 TM, and ±7.9 m for the SPOT image. These values illustrate the excellent geometric fidelity provided by both satellite systems.

But, notwithstanding the good overall accuracy, the rectification produced local misregistrations (1–1.5 pixels) that are due to the different resampling algorithms used for the respective system corrections. EURIMAGE produces system corrected TM data by applying the nearest neighbor resampling method. The same product is not available with cubic convolution resampling which, on the other hand, is routinely applied to generate SPOT level 1B CCTs (SPOT IMAGE, 1986).

Table 3. Landsat-5 TM and SPOT HRV-1 Dynamic Ranges in the Comparable Bands

Band	*0.5%*	*99.5%*	*Range*	*Range for $\theta = 42.0°$*
XS1	22	53	31	31
TM2	15	42	27	30
XS2	12	49	37	37
TM3	12	51	39	43
XS3	22	82	60	60
TM4	17	88	71	78

RADIOMETRIC COMPARISON AND SENSOR CALIBRATION

In our radiometric analysis of the TM and SPOT data, we used only pixel values from the system corrected, nongeocoded data sets at their respective original spatial resolution.

At first, comparable scene statistics and histograms were calculated for the total scene overlap, and for two subareas of dominantly forest and agricultural coverage. The dynamic ranges for each TM and SPOT band were then determined in relation to the 0.5 percentile and 99.5 percentile ranks of the histograms. In addition, a correction for the lower sun illumination has been applied to the TM data.

There were no significant differences between the SPOT XS1 and the TM2 spectral channel, but the comparison between TM 3/SPOT XS2 and TM 4/SPOT XS3 revealed a somewhat larger dynamic range of the Thematic Mapper data (Table 3). The same relation was obtained for the forested and agricultural subregions, which conforms to the results from previous comparisons (Verdin et al., 1987).

After its upward transmission through the atmosphere, the attenuated ground reflected solar irradiance is registered from the detectors of the optical sensor and transformed into an electric signal which is then amplified, digitized, encoded, and finally transmitted to the ground receiving stations. Many research and operational applications require the conversion of digital count values (DC) to quantitative physical values of at-satellite measured *radiance* or *reflectance* which can be retrieved from these digital counts (DC) by using a set of gain and bias pairs representing the calibration of the sensor.

Thematic Mapper radiances L_{tm} (mW/cm^2/sr/μm) for the bandpasses of its six reflective channels are obtained from the relation

$$L_{tm} = a_0 + a_1 \, DC, \tag{2}$$

and the at-satellite radiance L_{xs} (W/m^2/sr/μm) in the spectral channels of the SPOT HRVs is calculated with

$$L_{xs} = a_1^{-1}(m) \, DC, \tag{3}$$

where the gain factors have eight possible settings m, representing powers of the factor 1.3, then yielding

$$a_1(m) = a_1(m_0) \, 1.3^{m_0 - m}. \tag{4}$$

The header records of the SPOT scene used in this study indicate standard gain settings for all spectral bands ($m = m_0$).

SPOT calibration constants are updated monthly by using the on-board sun calibrator and provided on each CCT. In March 1986, this internal calibration device was tested at White Sands and, after some initial adjustments, a precision of $\pm 5.4\%$ was specified (Begni et al., 1986). The calibration of the XS1 and XS2 channels was then confirmed by a new series of measurements, but the calibration gain of the near-infrared bandpass (XS3) had to be increased by 8% (Begni, 1988). We have accordingly modified the XS3 gain factor

Table 4. Landsat-5 Thematic Mapper Calibration Updates[a]

Band	*Preflight*		*In-Flight Update*	
	a_0	a_1	a_0	a_1
TM1	−0.1009	0.0636	−0.1331	0.0727
TM2	−0.1919	0.1262	−0.2346	0.1385
TM3	−0.1682	0.0970	−0.1897	0.1102
TM4	−0.1819	0.0914	−0.1942	0.0885
TM5	−0.0398	0.0126	unchanged	unchanged
TM7	−0.0203	0.0067	unchanged	unchanged

[a]The coefficients are based on ground measurements performed at White Sands, New Mexico (Slater et al., 1986).

Table 5. Comparison of Modeled Thematic Mapper Reflectances (Dependent Variable) and Associated Ground Measurements (Independent Variable)

	ToA Reflectance				*Ground Reflectance*			
Band	a_0	a_1	r^2	*RMSE*	a_0	a_1	r^2	*RMSE*
TM1	.108	.515	.778	.017	.009	.829	.966	.009
TM2	.070	.617	.941	.011	.007	.973	.983	.009
TM3	.054	.659	.974	.011	.005	.967	.983	.009
TM4	.046	.813	.989	.012	.002	1.002	.994	.009

provided in the header information of our SPOT scene.

The Calibration of the Landsat-5 Thematic Mapper

The calibration gains (a_1) and offsets (a_0) of the Landsat-5 Thematic Mapper have been thoroughly assessed in the laboratory, but, during launch and later in orbit, each system undergoes stresses and environmental changes which may affect its radiometric performance. Its on-board calibration device can provide effective adjustments, but only if a decreasing system sensitivity is not due to a deterioration of the optical transmission. The quantitative use of satellite radiometry therefore suggests the need for verifying satellite measured radiances, and the TM in-flight calibration has been analyzed through a series of contemporary ground measurements at the large uniform gypsum sand area of White Sands, New Mexico (Slater et al., 1986; 1987).

We have used the results from these ground verification experiments to deduce a set post-launch calibration constants for the visible and near-infrared TM bands (TM1–TM4). Respective updates for the short-wave infrared bands appeared more ambiguous due to stronger variations of the measurement, and have not been used (Hill and Sturm, 1991). All updated calibration functions (Table 4) relate to band means and do not account for detector-to-detector response variations.

Reflectance-based assessments of the in-orbit calibration require detailed ground and atmospheric measurements near the overpass time of

Figure 2. Comparison of ground-measured and TM top-of-atmosphere (ToA) and modeled ground reflectance factors for various bare soil surfaces and agricultural crops obtained from Thematic Mapper data acquired over the Novara region (Italy) in 1988: (■) TM1; (□) TM2; (△) TM3; (⊠) TM4.

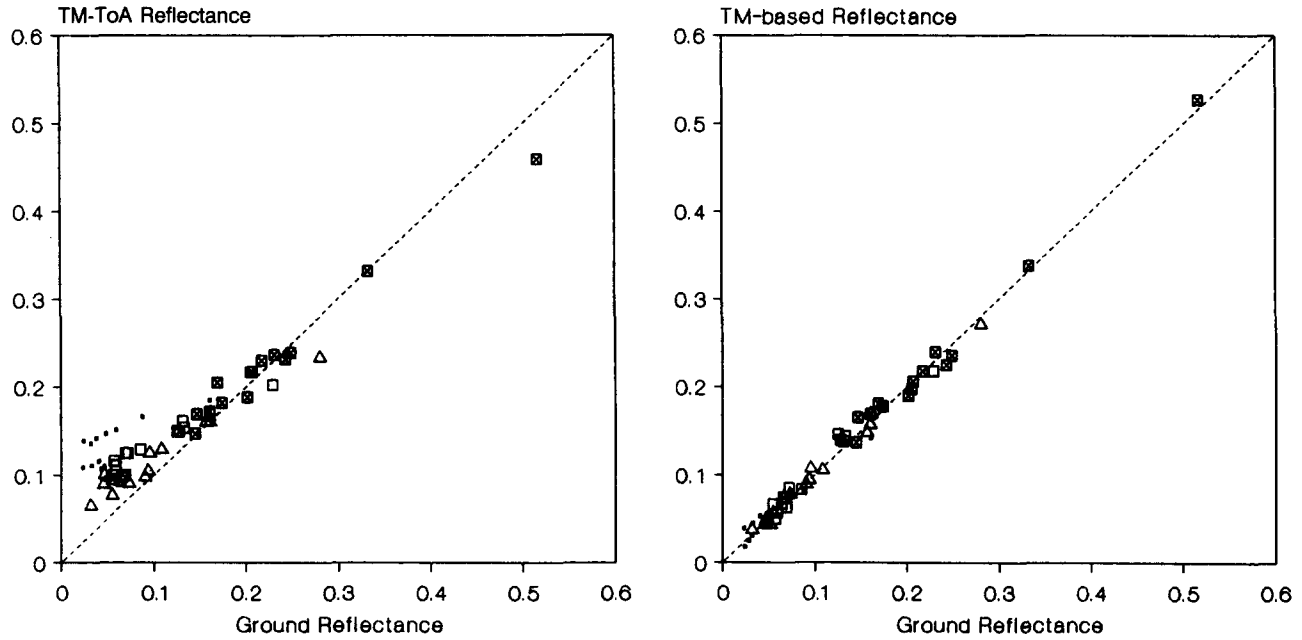

the satellite, and the use of radiative transfer computations to predict the radiance at the aperture of the satellite sensor, which is then compared to the corresponding digital counts. In our experiments we used a model which is based on the formulation of radiative transfer as developed from Tanré et al. (1979; 1985). The code provides corrections for atmospheric scattering, absorption, and pixel adjacency effects, and it makes extensive use of analytical expressions and preselected atmospheric models, resulting in a high precision and a short execution time. It directly relates the apparent at-sensor reflectance ρ^* to the target reflectance factor ρ_t, according to

$$\rho^* = t_g(\mu)\left\{\rho_{at} + \frac{T(\mu_0)[t_d(\mu)\rho_t + t_s(\mu)\langle\rho\rangle]}{1-\langle\rho\rangle s}\right\}, \quad (5)$$

where ρ_t is the target reflectance, $\langle\rho\rangle$ the background contribution to the apparent reflectance, and s gives the spherical albedo; ρ_{at} denotes the intrinsic atmospheric signal component, and μ and μ_0 are the cosines of the zenith angles of the direction vectors from the pixel towards satellite and sun. $T(\mu_0)$ gives the total downward, $t_d(\mu)$ the diffuse, and $t_s(\mu)$ the scattered upward transmittance; $t_g(\mu)$ denotes the upward gaseous transmittance of the atmosphere (Tanré et al., 1987).

Based upon this model, the validity of the updated TM calibration constants was first confirmed by an experiment that involved ground-based monitoring of atmospheric conditions and the spectral radiance of a flat and homogeneous ground target at the time of a Landsat-5 TM overflight in 1984 (Maracci et al., 1986; Hill and Sturm, 1991). As part of an additional ground radiometry campaign in 1988, atmospheric and target reflectance measurements were carried out during three different TM overpasses in the vicinity of the Joint Research Centre (Maracci et al., 1990). The comparison of the top-of-atmosphere (ToA) and ground-measured target reflectance factors exhibited typical distortions which are due to atmospheric effects, but the atmospheric corrections produced a remarkably good coincidence between satellite- and ground-measured reflectance factors (Table 5, Fig. 2). All regression lines are well defined, the intercepts appear negligible, and the slopes for TM2, TM3, and TM4 spectral channels approach the ideal 1-to-1 relation. It appears that no significant degradation of the TM system response has occurred during this period. Only the regression result for the TM1 band may suggest an erroneous calibration, but it cannot be excluded that its deviation from the 1-to-1 relation is due to shortcomings of the atmospheric correction method.

Comparison of TM and SPOT In-Flight Calibrations

Having obtained these results from the reflectance-based analysis of TM scenes acquired in 1984 and 1988, we tried to further corroborate the updated TM calibration coefficients by a comparison between our coincident SPOT and TM images from 1986. In the case of almost simultaneous data acquisitions from space orbits, the comparison of different satellite measurements does not require radiative transfer calculations, once the atmospheric conditions have been sufficiently stable.

The assumption of a stable atmosphere during the SPOT and TM overpasses seems to be confirmed by the analysis of ToA reflectances from water targets included in both data sets (Fig. 3). In the case of a noticeable change in atmospheric

Figure 3. Top-of-atmosphere reflectance factors for various clear water targets obtained from simultaneously acquired Thematic Mapper and SPOT HRV-1 data (Ardèche, France, 29 September 1986): (——) TM (average); (□) TM; (△) SPOT.

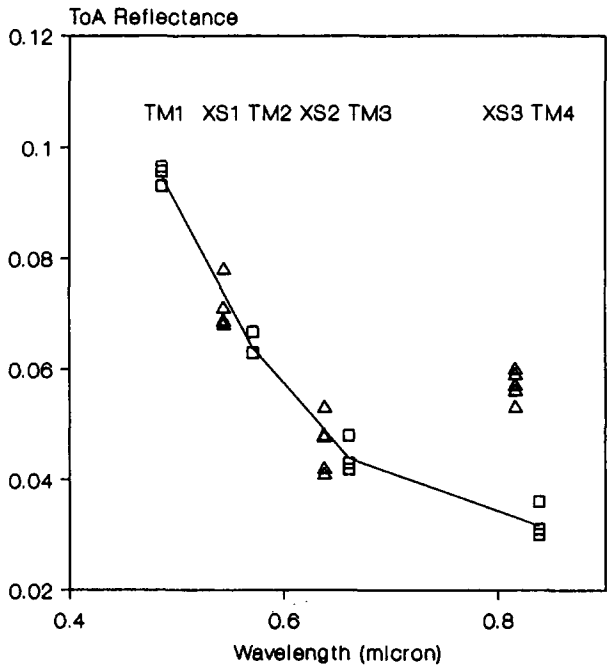

reflectance, especially the XS1 and XS2 reflectances should significantly deviate from the TM reference. For the comparison of the TM and HRV-1 in-flight calibration we have therefore used the apparent at-satellite reflectance ρ^*, which still represents the combined earth–atmosphere system, but provides a compensation for differences in illumination geometry. Assuming lambertian ground reflectance, the apparent (or top-of-atmosphere) reflectance can be computed for a given spectral band with

$$\rho^* = \frac{\pi L d^2}{E_0 \cos(\theta_0)}, \qquad (6)$$

where θ_0 is the solar zenith angle and d is a correction coefficient for the actual sun–earth distance. The exoatmospheric solar irradiance E_0 for the Thematic Mapper and SPOT HRV-1 bandpasses (Table 1) is provided by Markham and Barker (1987) and Price (1988), and the retrieval of at-satellite measured spectral radiances L from the digital counts (DC) involves the use of respective calibration functions.

In order to compare both Landsat-5 TM and SPOT HRV-1 calibration, we used 39 carefully selected reference sites which were all located on flat terrain in order to minimize effects due to the different sun illumination. The average size of these reference targets was about 40 pixels on SPOT, and 18 pixels on TM spatial resolution, and the digital counts covered most of the TM and SPOT dynamic range. The spectral variation within the target areas was adequately low: average coefficients of variation for the visible and near-infrared TM bands amount only to 3.1%, 5.0%, 6.8% and 5.4% of the mean signal.

We then tried to use the TM signal from these sites to simulate the corresponding HRV radiances. The average TM grey level count (DC_{tm}) of each target was first converted into apparent reflectance ρ_{tm} [(Eq. 6)] by using the updated Thematic Mapper calibration coefficients (Table 4). Then it was attempted to reconstruct a continuous TM top-of-atmosphere spectrum by means of polynomial interpolations (Press et al., 1986), using the signal as measured in its discrete visible and near-infrared bands (TM1-TM4). There is in fact solid evidence that such interpolated spectra, especially for bare soils, are close in form to the true situation (Fig. 4).

The simulated apparent SPOT reflectances ρ^*_{xs} were finally obtained by an integration of the

Figure 4. (a) Comparison of a continuous reflectance signature of bare soil acquired with the SE-590 radiometer (2.5 nm sampling interval) and the resulting interpolation using this signal at the wavelength of the visible and near-infrared TM bands. Figure 4(b) presents continuous soil, vegetation, and water signals produced by the polynomial interpolation of Thematic Mapper top-of-atmosphere reflectance factors from the Ardèche data.

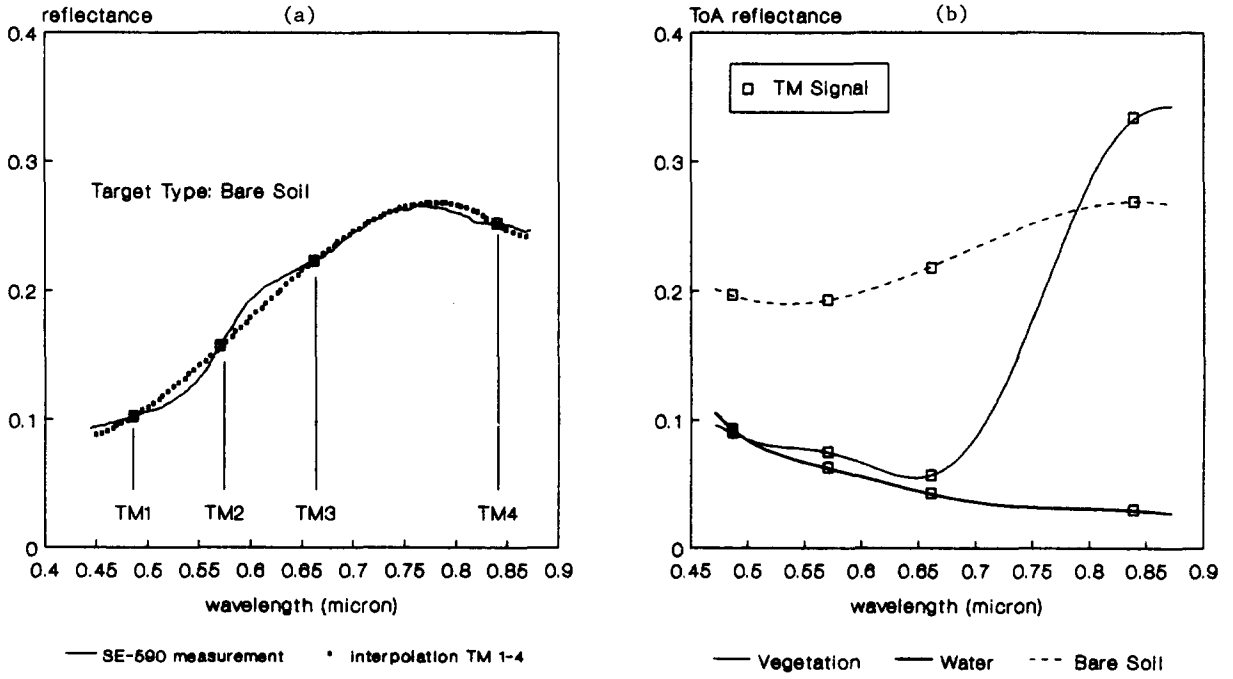

continuous TM ToA-spectra (obtained from the interpolation) within the effective bandwidth of the HRV-1 bandpasses (SPOT IMAGE, 1986). The spectral response function ϕ for each HRV channel was approximated by a gaussian fit, normalized to peak response, and the simulated band-averaged SPOT ToA-reflectance in the respective wavelength interval λ_0 to λ_1 was finally computed with

$$\rho^{*\prime}_{xs} = \int_{\lambda_0}^{\lambda_1} d\lambda\, \rho_i^* \phi, \qquad (7)$$

where ρ_i^* denotes the interpolated apparent reflectance in the spectral smapling interval $d\lambda$. TM-based SPOT radiances L'_{xs} were readily obtained by inverting Eq. (6), and the corresponding TM-based calibration function for each HRV bandpass has been determined through a linear regression analysis between TM-simulated HRV-radiances and HRV digital counts, using our sequence of homogeneous reference targets.

Spectral signatures from bare soil, vegetation, and water targets were used for the comparative analysis of the visible bands. The regression analysis of the near-infrared signals, however, was exclusively based upon spectra from bare soils because interpolation methods usually fail to adequately represent the top-of-atmosphere signal around the vegetation red edge. Water signals were excluded in order to minimize the impact of TM calibration errors on the resulting regression slope.

All regression lines (Fig. 5) have a high coefficient of determination (0.996, 0.997, and 0.988), and the root mean square (RMS) radiance differences for the three bands ($\pm$0.120, 0.154, and 0.160) are very small. The slopes of the TM-based HRV calibration functions agree within 5.9% (XS1), 4.0% (XS2), and 2.1% (XS3) to the SPOT in-flight calibration gains; the intercepts of the XS1 and XS2 spectral bands (0.088, $-$0.064) correspond to less than 1 digital count and are therefore considered negligible. Only for the near-infrared channel (XS3), our regression analysis produced a significant intercept ($-$0.287) in the magnitude of 3 digital counts. This term could be due to uncertainties of the TM calibration update or the interpolation method, but, given the good determination of the regression line, it might in fact indicate the existence of a residual dark current.

Figure 5. Comparison of TM-based (—) and SPOT HRV-1 [--- (CCT)] in-flight calibration functions for the XS1, XS2, and XS3 spectral bands (water targets not used in regression analysis).

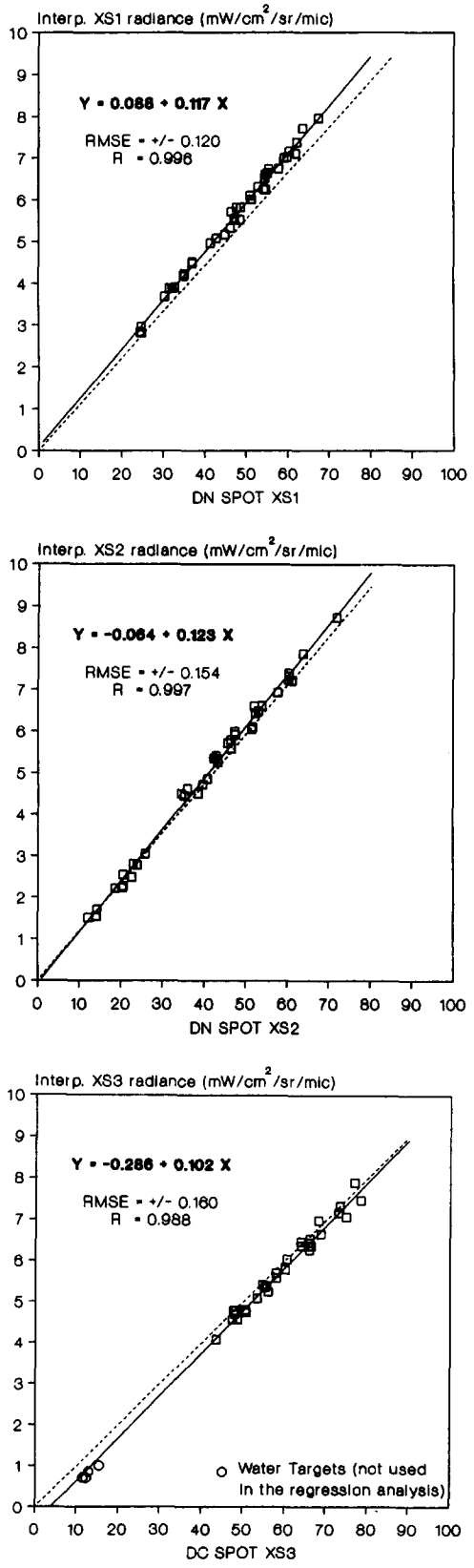

The surprisingly good coincidence between the TM-based calibration gains of the SPOT HRV-1 and the constants provided by its own on-board calibrator (Table 6) is understood as a confirmation of the in-flight calibration of both systems. In the context of the various ground-based calibration assessments mentioned above we conclude that, after some initial alteration during the satellite's launch, TM calibration has been remarkably stable throughout the period from 1984 to 1988. Our results equally give evidence of the good precision that was achieved in the reflectance-based calibration assessments and updates (Slater et al., 1986; 1987; Begni et al., 1986; Begni, 1988), and it emphasizes the importance of such approaches for the quantitative use of satellite data.

Table 6. TM-Based and CCT (In-Flight) Calibration Gains for the SPOT HRV-1 (Ardèche, 29 September 1986), Radiance ($mW/cm^2/sr/\mu m$)

Band	*n*	r^2	*TM-Based RMSE*	a_0	a_1	*SPOT CCT a*
XS1	39	.987	±.120	.0878	.1167	.1105
XS2	39	.997	±.154	−.0642	.1234	.1183
XS3	30	.988	±.160	−.2865	.1023	.0999

THE COMPARISON OF SPECTRAL FEATURES

In numerous remote sensing applications, greenness and brightness indicators (vegetation indices, Tasseled Cap features) have proven their suitability to emphasize important object characteristics. Field experiments have demonstrated that key parameters such as leaf area index, absorbed photosynthetic active radiation, and wet and/or dry biomass are related to the normalized difference vegetation index (NDVI) or similar combinations of wavebands in the visible and near-infrared. The assessment of such variables is therefore of specific interest to applications in agriculture and vegetation monitoring.

The quantitative use of spectral greenness and brightness features in multiple sensor approaches depends above all on a reliable sensor calibration (Price, 1987), but it also requires that the waveband dependent differences between the various systems are well understood. It results from simulation studies which used extensive radiometric field measurements that the vegetation indices (NDVI) from the NOAA-AVHRR sensors are linearly related to those obtained from Landsat TM and SPOT HRV wavebands (Gallo and Daughtry, 1987). This implies that a linear relationship exists between the TM and SPOT vegetation indices.

An image-based verification of these interdependences is of great importance for multiple-sensor approaches since the resulting functions are needed to mutually adjust the corresponding spectral indices. We have therefore attempted to validate the results of Gallo and Daughtry (1987) by comparing the NDVI scores which were derived from the contemporarily acquired SPOT and TM images. In addition to that, we have analyzed the "Tasseled Cap"-like greenness and brightness indicators from both sensor systems.

Atmospheric Corrections

Since these spectral indices are obtained from channel ratios or linear band combinations, they are sensitive to atmospheric attenuation (Jackson et al., 1983). In order to directly compare our results to those that Gallo and Daughtry (1987) had obtained from their radiometric field data, both TM and SPOT scenes had to be corrected for atmospheric effects [Eq. (5)].

The atmospheric conditions during the TM overpass were estimated by using clear water as reference target. Once appropriate corrections of the environmental scattering effects are applied (Tanré et al., 1987), even small water surfaces of approximately known reflectance can be successfully adopted for an estimate of atmospheric conditions (Royer et al., 1988; Hill and Aifadopoulou, 1989). The aerosol optical depth is then determined from scene data by an iterative approach which converges as soon as the modeled apparent reflectance of the target is equal to the scene-measured value of ρ^*.

Table 7. Scene-Estimated Atmospheric Conditions: TM Ardèche 29 September 1986, 9.49 h GMT

	TM1	*TM2*	*TM3*	*TM4*	*TM5*	*TM7*
τ_r	.1657	.0862	.0473	.0179	.0010	.0003
τ_a	.4108	.3419	.2829	.1647	.0785	.0463
ρ_{at}	.0946	.0552	.0347	.0174	.0035	.0021
$T(\mu_0)$	.7744	.8504	.8957	.9394	.9894	.9905

$\tau_a = .13\lambda^{-1.68}$, with $r^2 = -0.985$

τ_r = molecular optical depth; τ_a = aerosol optical
ρ_{at} = atmospheric reflectance; $T(\mu_0)$ = downward transmittan

Table 8. Scene-Estimated Atmospheric Conditions: SPOT Ardèche 29 September 1986, 10.47 h GMT

	XS1	*XS2*	*XS3*
τ_r	.1048	.0546	.0200
τ_a	.3114	.2345	.2395
ρ_{at}	.0582	.0365	.0205
$T(\mu_0)$	.8603	.8989	.9307
$\tau_a = .20\lambda^{-0.59}$, with $r^2 = -0.756$			

With a horizontal visibility of 13.9 km, the resulting estimate indicates relatively hazy atmospheric conditions (Table 7). It was difficult to obtain an independent estimation from the SPOT scene: using CCT calibration gains, the estimated optical depth in the near-infrared exceeded even the XS2 estimate, and the resulting Angstrom relation was badly defined (Table 8). We therefore used the TM-based estimation of the atmospheric transmission for the correction of both scenes; the effects of gaseous absorption due to atmospheric water vapor and ozone were accounted for with LOWTRAN standard (midlatitude–summer) atmospheric data. Such scene-based atmospheric corrections usually permit us to retrieve surface reflectance factors with a precision of better than ± 0.02 reflectance units (Hill and Aifadopoulou, 1989).

In order to assess the influence of minor calibration differences we processed the SPOT data with both in-flight and TM-based calibration coefficients.

The Normalized Difference Vegetation Index (NDVI)

A green leaf's chlorophyll pigment strongly absorbs solar radiation at wavelengths between 0.5 μm and 0.7 μm (visible red) and the reflectance factor is normally below 0.1. In the near-infrared region (0.75–1.35 μm), multiple scattering occurs due to the leaf's internal mesophyll structure and the reflectance tends to be in the range of 0.4–0.6. This physiological relationship has been used to estimate the greenness of plant canopies through the use of various ratios (i.e., simple ratio NIR/R, normalized difference NIR − R/NIR + R).

We primarily assessed the relation between TM and SPOT vegetation indices by a regression analysis which relates to more than 40 reference areas. For each of these targets, SPOT and TM vegetation indices were calculated based on the retrieved ground reflectance ρ_t in the corresponding channels of the visible red and the near-infrared. Since the band ratioing involved in the calculation of the NDVI considerably reduces the spectral variations due to surface topography and sun elevation (Holben and Justice, 1981), an additional method has been applied which was originally designed for radiometric scene normalization (Schott et al., 1988). Assuming that the NDVI distributions from the overlapping scene areas are linearly related, the $NDVI_{tm}$ from Thematic Mapper data can accordingly be transformed to equivalent SPOT vegetation indices $NDVI_{xs}$ with

$$NDVI_{xs} = \frac{\sigma_{xs}}{\sigma_{tm}} NDVI_{tm} + \left[\overline{NDVI}_{xs} - \frac{\sigma_{xs}}{\sigma_{tm}} \overline{NDVI}_{tm}\right], \quad (8)$$

where $\overline{NDVI}_{xs}$ and $\overline{NDVI}_{tm}$ are the means of the NDVI distributions derived from the geometrically registered and atmospherically corrected SPOT and TM images and σ_{xs} and σ_{tm} denote the respective standard deviations.

Both target- and histogram-based relations do in fact corroborate the results of Gallo and

Figure 6. SPOT HRV-1 NDVI frequency histogram produced by using CCT (—) and TM-based (—) calibration coefficients (the corresponding Thematic Mapper NDVI frequency histogram from the overlapping image area is represented by vertical bars).

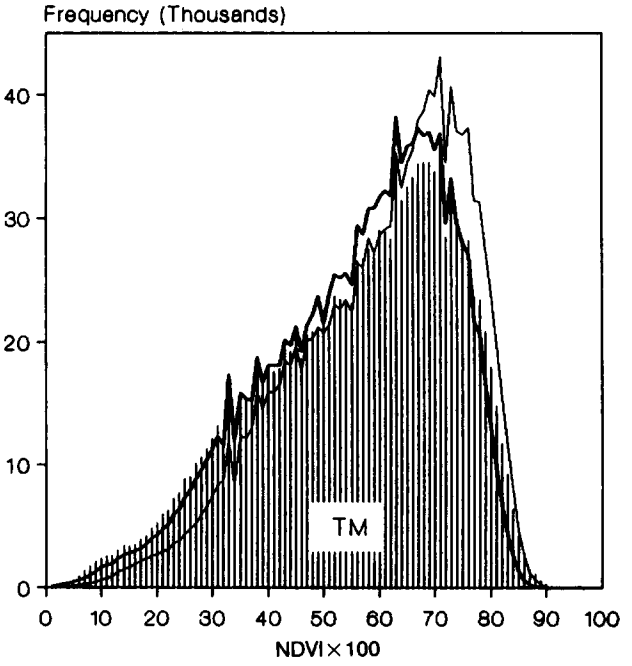

Table 9. Coefficients of the Linear Relationships Between the NDVI of the Landsat-5 TM and the SPOT HRV-1 Systems (T = from Reference Targets, H = from Histogram Comparison)

	Dependent Variable: XS				*Dependent Variable: TM*				
	a_0	a_1	r^2	*RMSE*	a_0	a_1	r^2	*RMSE*	*Spot Calibration*
T	.073	.907	.998	.017	−.079	1.100	.998	.016	in-flight
H	.095	.898			−.105	1.113			in-flight
T	.032	.932	.998	.016	−.033	1.071	.999	.017	TM-based
H	.036	.935			−.037	1.067			TM-based
Meas.[a]	.040	.953	.999	.007	−.042	1.049	.999	.007	

[a]From spectral ground measurements (Gallo and Daughtry, 1987).

Daughtry (1987): once TM-based calibration gains are used for processing the HRV-1 data, the relation between TM and SPOT NDVI scores compares almost perfectly to the results obtained from the radiometric field data (Table 9). The difference in low range (< 0.2) is only 6–7%, and high NDVI scores (0.6–0.8) deviate only by 3% from the expected values. It is in accordance with the dynamic range of the corresponding spectral bands that the NDVI from the SPOT system occupies a slightly smaller range than the TM-based index (Fig. 6).

The use of SPOT in-flight calibration gains produced a reflectance-based NDVI distribution which somewhat deviates from the ground-measured relation (Table 9). In its low range, the SPOT vegetation index exhibits an offset towards higher NDVI scores. Due to the NDVI saturation which becomes evident above 0.80, this leads to a compression of the total value range (Fig. 6).

It follows that calibration gain differences of less than 5% can produce variations of low range NDVI scores (< 0.2) which amount to 10–20%. This illustrates the need for an adequate monitoring of the in-flight calibration of optical satellite instruments which might be used in multiple sensor approaches (Fig. 7).

Landsat-TM and SPOT Tasseled Cap Features

The Tasseled Cap transformation of Landsat Thematic Mapper data produces three spectral features known as "brightness," "greenness," and "wetness." It preserves euclidean relationships in the data space, and captures typically more than 95% or more of the total data variability (Crist and Cicone, 1984). Thus it provides a mechanism for data reduction and enhanced data interpretability by emphasizing structures in the spectral data which are due to physical characteristics of dominant scene classes (Crist, 1985).

This type of transformation is intended to be an invariant process which can be applied to any TM scene, but atmospheric effects will affect the results as long as count-related transformation coefficients are used to transform uncorrected imagery. Therefore, a transformation matrix has been developed which converts reflectance factor data to TM Tasseled Cap equivalent features (Crist, 1985). As an alternative, site-specific coefficients can be obtained from suitable scene spectra (bare soil, vegetation and water) using the Gram–Schmidt orthogonalization process (Jackson, 1983).

Both concepts have been applied to transform the atmospherically corrected TM data. It is found that the scene-based transformation of the TM reflectance data reveals characteristics of a principal component transformation (variance decreases with the rank of features). The brightness and greenness distributions obtained with the two approaches are found in close correspondence, but shape and dynamic range of the reflectance-based wetness histogram indicate that slightly different information is contained in this feature (Fig. 8). It is probably due to the methodological difference in defining the brightness axis (Crist and Cicone, 1984; Jackson, 1983) that more information is present in the third feature of the standard Tasseled Cap transformation (Crist, 1985).

Due to the reduced data dimensionality, equivalent transformations of SPOT HRV and corresponding three-band TM data will generally not produce valuable wetness features. It is therefore expected that the Gram–Schmidt orthogonalization provides an almost optimum set of transformation coefficients. The transformation matrix for the SPOT compatible spectral subset of TM (TM2–TM3–TM4) was consequently derived by

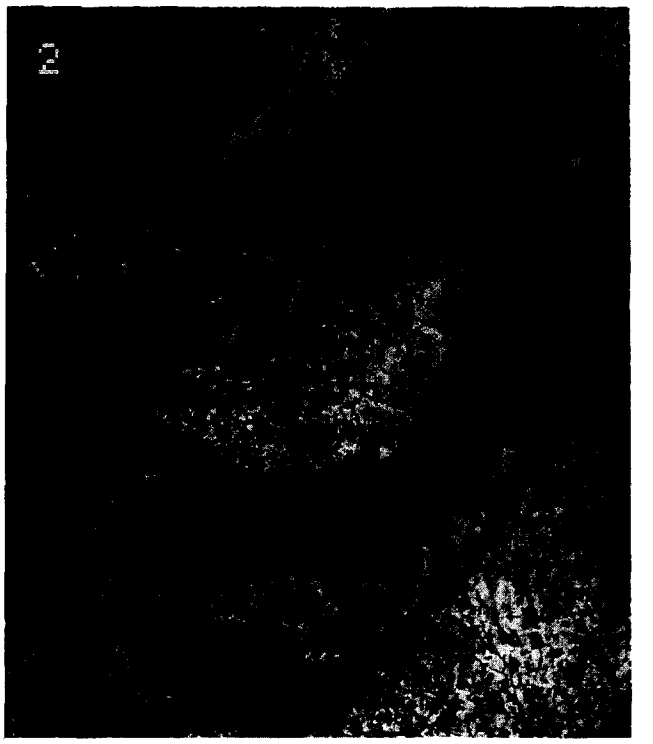

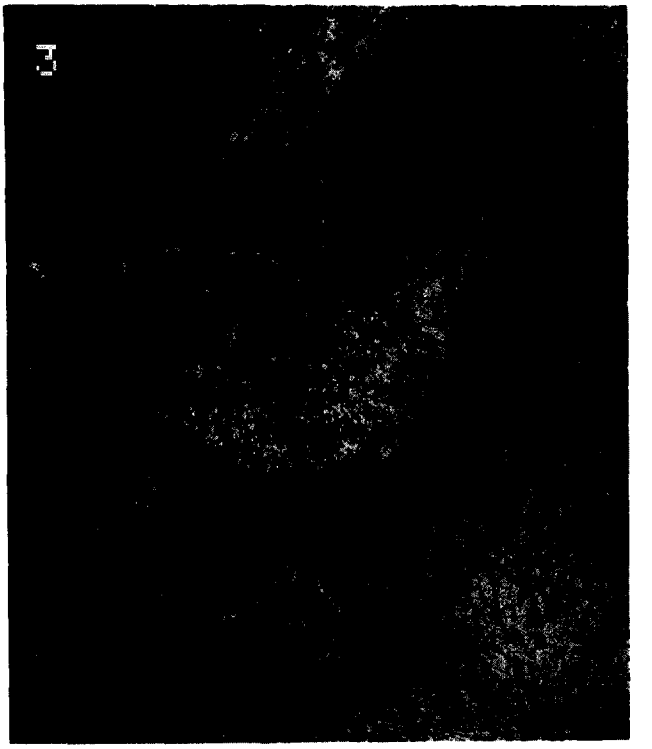

Figure 7. A representative part of the study region is shown as a geocoded colour composite of the Thematic Mapper Bands 4 (red), 5 (green), and 3 (blue) (1). The normalized difference vegetation index (NDVI) as derived from TM data is given in (2). Once the experimentally retrieved relation between SPOT- and TM-based normalized vegetation indices (Gallo and Daughtry, 1987) is used to transform the SPOT NDVI scores to TM-equivalent values, both data sets are found in good agreement (3).

Table 10. Scene-Based Tasseled Cap Equivalent Transformation Matrices for Landsat-5 TM (TM1–TM5, TM7), SPOT, and the Corresponding Landsat-5 TM Spectral Subset (TM2–TM3–TM4) Reflectance Factor Data

Feature	*TM1*	*TM2*	*TM3*	*TM4*	*TM5*	*TM7*
BR	.2142	.4284	.5315	.4601	.4363	.2935
GR	−.1383	−.1134	−.2694	.8758	−.2334	−.2718
W	.0591	.5808	.3272	−.1111	−.5647	−.4699
Feature	*TM2*	*TM3*	*TM4*	*XS1*	*XS2*	*XS3*
BR	.5204	.6456	.5589	.4767	.6554	.5859
GR	−.2783	−.4905	.8252	−.3037	−.5027	.8094
W	.8073	−.5853	−.0756	.8250	−.5637	−.0406

using the same spectral signatures which had already been adopted to define the site-specific coefficients used in the previous comparison. The corresponding coefficient matrix for the transformation of SPOT HRV data was then obtained by an interpolation of the TM reflectance spectra (Table 10).

Based upon our results from the NDVI comparison, we only used TM-based calibration gains for processing the SPOT HRV data. The resulting brightness and greenness histograms appear similar, in which the SPOT features exhibit once more a somewhat smaller dynamic range than those obtained from TM (Fig. 9). The third feature of related, and it is concluded that also these target-characterized by a distinctly reduced variance, and system-specific noise patterns dominate the image (Fig. 10). Any quantitative assessments, however, had to be restricted to our reference targets since the differences in terrain illumination introduce such great variations that valid histogram comparisons could be obtained only for very small subregions. The target-based analysis uses absolute scores as they result from applying the transformation coefficients to the reflectance factors. Again, the Tasseled Cap equivalent brightness and greenness features of SPOT and TM are linearly

Figure 8. Frequency histograms of TM Tasseled Cap brightness, greenness, and wetness features as a function of adopting standard (Crist, 1985) (—) or site-specific (—) transformation coefficients.

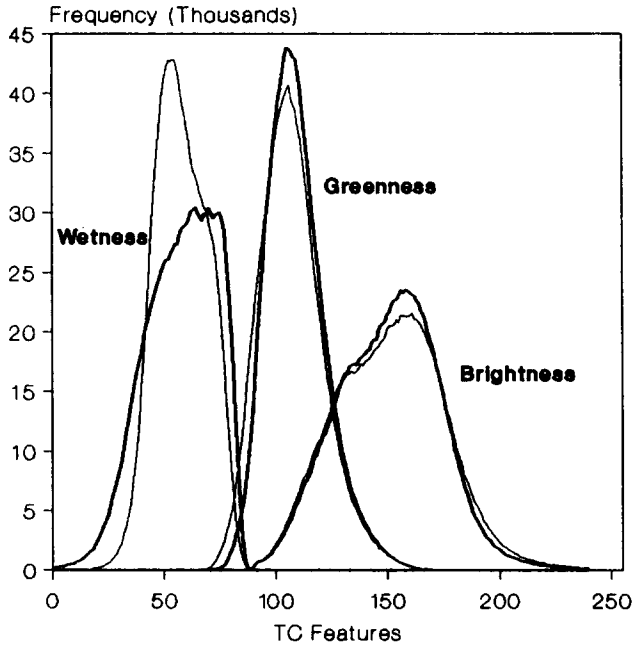

Figure 9. Comparison of the SPOT (XS1–XS2–XS3) (—) Tasseled Cap brightness and greenness frequency histograms with the corresponding features from six- (TM1–TM5, TM7) (- - ·) and three-band TM (TM2–TM3–TM4) (—) Tasseled Cap transformations.

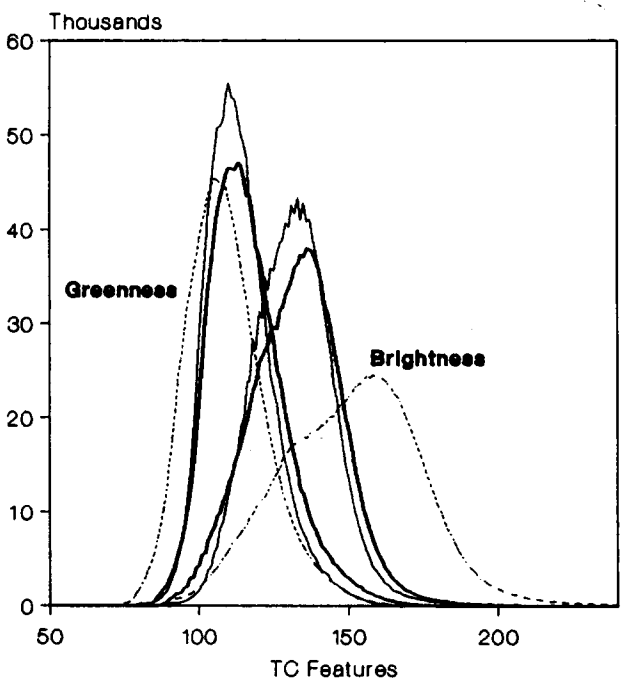

Table 11. Coefficients of the Linear Relationships between the Reflectance-Based Tasseled Cap Equivalent Features from SPOT HRV-1 and three-band (TM2–TM3–TM4) Landsat-5 Thematic Mapper Data

	Dependent Variable: XS				*Dependent Variable: TM*			
	a_0	a_1	r^2	*RMSE*	a_0	a_1	r^2	*RMSE*
BR6	.039	.559	.974	.029	−.045	1.698	.974	.050
GR6	.065	.696	.942	.029	−.078	1.276	.942	.039
BR3	.014	0.892	.994	.013	−.012	1.108	.994	.015
GR3	.008	.864	.995	.009	−.008	1.147	.995	.010

Figure 10. Tasseled Cap equivalent brightness, greenness, and wetness features derived from six- and three-band TM and SPOT imagery.

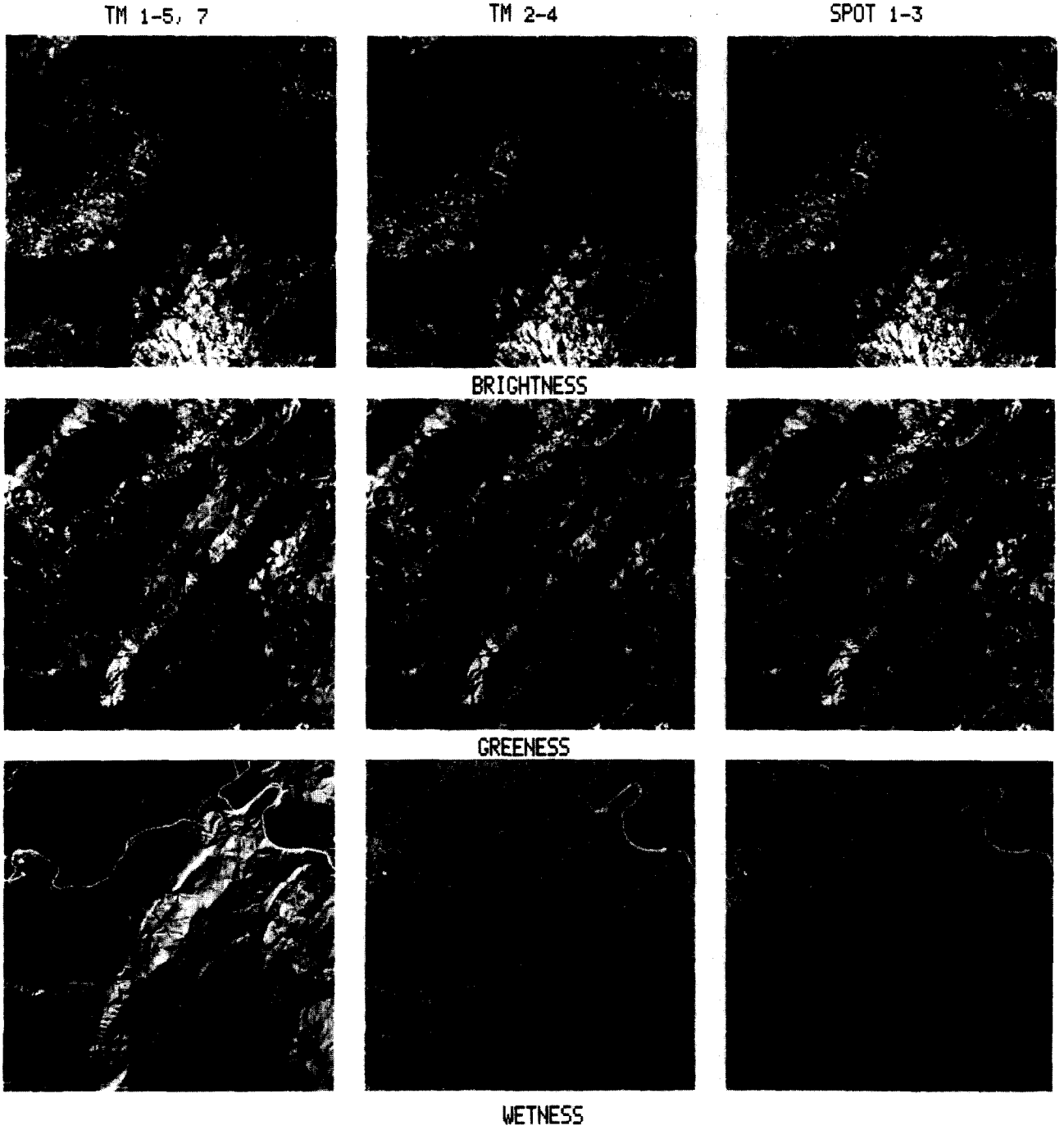

the transformed TM and SPOT data is in fact based relations can be used for mutual data adjustments (Table 11).

CONCLUSIONS

Landsat-5 TM and SPOT HRV-1 data can be registered to a common map grid of 30 m×30 m ground resolution with subpixel accuracy, but, in order to account for mountainous relief, digital elevation data should be associated with the correction process.

A method for comparing of radiometric sensor characteristics by use of contemporarily acquired imagery of the same region was successfully tested, and it has confirmed the in-flight calibration of both SPOT and TM systems in 1986. Comparing the visible bands of the HRV-1 instrument with the coincident TM scene, revealed only minor discrepancies which amount to less than 5% of SPOT in-flight calibration gains. The calibration adjustment for the near-infrared band (XS3) that was communicated from SPOT IMAGE (Begni, 1988), is clearly confirmed by our comparative analysis, but there was also some evidence for the existence of an instrument related offset term to be applied to the near-infrared band of the HRV-1 sensor.

The TM in-flight calibration coefficients, which were deduced from results of the ground measurement campaign at White Sands (Slater et al., 1986), have provided good results. We have meanwhile used these calibration coefficients with Landsat-5 TM data from 1984, 1988, and now 1986, and the resulting count-to-reflectance conversions emphasize that they provide a valuable alternative to the use of in-flight calibration data. It is thereby suggested that TM may be used as calibration reference for further evaluations of this type.

TM and SPOT data permit a quantitative analysis in terms of ground reflectances, once suitable calibration data are provided. It is due to the differences in central wavelength and equivalent bandwidth of the corresponding spectral channels that both systems provide slightly different brightness and greenness information (Tasseled Cap equivalent brightness and greenness, normalized difference vegetation index). But these indices are linearly related, and the associated transfer functions permit mutual data adjustments. Therefore, a wide range of applications in agricultural monitoring and vegetation observation can be approached by using multiple sensor data sets which involve TM and SPOT imagery.

REFERENCES

Begni, G. (1988), Absolute calibration of Spot data, *Spot Newsletter* 10:2–3.

Begni, G., Dinguirard, M. C., Jackson, R. D., and Slater, P. N. (1986), *Absolute Calibration of the SPOT-1 HRV Cameras*, SPIE Vol. 660, pp. 66–76.

Bernier, M., Cihlar, J., Dupont, O., and Moreau, S. (1988), Analyse spectrale comparative des capteurs HRV et TM, *Can. J. Remote Sens.* 14(2):118–123.

Chavez, P. S., Jr., and Bowell, J. A. (1988), Comparison of the spectral information content of Landsat Thematic Mapper and SPOT for three different sites in the Phoenix, Arizona region, *Photogramm. Eng. Remote Sens.* 54(12):1699–1708.

Cliche, G., Bonn, F., and Teillet, P. M. (1985), Integration of the SPOT panchromatic channel into its multispectral mode for image sharpness, *Photogramm. Eng. Remote Sens.* 51(3):311–316.

Crist, E. P. (1985), A TM Tasseled Cap equivalent transformation for reflectance factor data, *Remote Sens. Environ.* 17:301–306.

Crist, E. P., and Cicone, R. C. (1984), A physically-based transformation of Thematic Mapper data—the TM Tasseled Cap, *IEEE Trans. Geosci. Remote Sens.* GE-22(3):256–263.

Gallo, K. P., and Daughtry, C. S. T. (1987), Differences in vegetation indices for simulated Landsat-5 MSS and TM, NOAA-9 AVHRR, and SPOT-1 sensor systems, *Remote Sens. Environ.* 23:439–452.

Haydn, R., Dalke, G. W., Henkel, J., and Bare, J. E. (1982), Application of the IHS color transform to the processing of multisensor data and image enhancement, in *Proc. International Symposium on Remote Sensing of Arid and Semi-Arid Lands*, Cairo, Egypt, pp. 599–616.

Hill, J., and Aifadopoulou, D. (1989), Scene-based atmospheric correction of Thematic Mapper imagery acquired during 1988 over the Ispra/Novara region, Italy, JRC Ispra, Inst. for Remote Sensing Appl., Technical report, available from the authors, 69 pp.

Hill, J., and Mégier, J. (1988), Regional land cover and agricultural area statistics and mapping in the Département Ardèche, France, by use of Thematic Mapper data, *Int. J. Remote Sens.* 9(9/10):1573–1595.

Hill, J., and Sturm, B. (1991), Radiometric corrections of multi-temporal Thematic Mapper data for the use in land-

cover classification and vegetation monitoring, *Int. J. Remote Sens.* forthcoming.

Holben, B. N., and Justice, C. O. (1981), An examination of spectral band ratioing to reduce the topographic effect on remotely sensed data, *Int. J. Remote Sens.* 2:115.

Jackson, R. D. (1983), Spectral indices in *n*-space, *Remote Sens. Environ.* 13:409–421.

Jackson, R. D., Slater, P. N., and Pinter, P. J. (1983), Discrimination of growth and water stress in wheat by various vegetation indices through clear and turbid atmospheres, *Remote Sens. Environ.* 13:187–208.

Kohl, H. G., and Hill, J. (1988), Geometric registration of multi-temporal TM data over mountainous areas by use of a low resolution digital elevation model, in *Proc. 8th EARSeL Symp. on Alpine and Mediterranean Areas: A Challenge for Remote Sensing*, Capri (Naples), Italy, 17–20 May 1988, pp. 323–335.

Maracci, G. C., Hosgood, B., and Andreoli, G. (1986), Measurements of spectral signatures in less favoured areas (LFA): a contribution to the definition of a remote sensing multi-temporal experiment, in *ESA / EARSeL Symp. on Europe from Space*, Lyngby, Denmark, 25–28 June 1986, ESA SP-258, pp. 215–218.

Maracci, G. C., Hosgood, B., Andreoli, G., and Grassi, P. (1990), Varese/Novara 88: field radiometry, Technical Note T.N.I. 90.05, Commission of the European Communities, JRC Ispra, Inst. for Remote Sensing Applications.

Markham, B. L., and Barker, J. L. (1987), Thematic Mapper bandpass solar exoatmospheric irradiances, *Int. J. Remote Sens.* 8(3):517–523.

Marvin, J. W., Labovitz, M. L., and Wolfe, R. E. (1987), Derivation of a fast algorithm to account for distortions due to terrain in earth-viewing satellite sensor images, *IEEE Trans. Geosci. Remote Sens.* GE-25(2):244–251.

Moran, M. S., Jackson, R. D., Hart, G. F., Slater, P. N., Bartell, R. J., Biggar, S. F., and Santer, R. P. (1987), Surface reflectance factors derived from SPOT-1 HRV data at two view angles, in *Proc. Int. Conference on SPOT 1, Image Utilization, Assessment, Results*, Paris, 23–27 November 1987, Cepadues, Paris, pp. 1365–1370.

Press, W. H., Flannery, B. P., Teukolsky, S. A., and Vetterling, W. T. (1986), *Numerical Recipes: The Art of Scientific Computing*, Cambridge University Press, Cambridge, New York, New Rochelle, Melbourne, Sydney.

Price, J. C. (1987), Calibration of satellite radiometers and the comparison of vegetation indices, *Remote Sens. Environ.* 21:15–27.

Price, J. C. (1988), An update on visible and near infrared calibration of satellite instruments, *Remote Sens. Environ.* 24:419–422.

Royer, A., Charbonneau, L., and Teillet, P. M. (1988), Interannual Landsat-MSS reflectance variations in an urbanized temperate zone, *Remote Sens. Environ.* 24:423–446.

Schott, J. R., Salvaggio, C., and Volchok, W. J. (1988), Radiometric scene normalization using pseudoinvariant features, *Remote Sens. Environ.* 26:1–16.

Slater, P. N., Biggar, S. F., Holm, R. G., Jackson, R. D., Mao, Y., Moran, M. S., Palmer, M., and Yuan, B. (1986), Absolute radiometric calibration of the Thematic Mapper, *SPIE* 660:2–8.

Slater, P. N., Biggar, S. F., Holm, R. G., Jackson, R. D., Mao, Y., Moran, M. S., Palmer, M., and Yuan, B. (1987), Reflectance- and radiance-based methods for the in-flight calibration of multi-spectral sensors, *Remote Sens. Environ.* 22:11–37.

SPOT IMAGE (1986), *Guide des Utilisateurs de données SPOT*, Révision No. 01 (December 1988), CNES, Toulouse.

Tanré, D., Herman, M., Deschamps, P. Y., and de Leffe, A. (1979), Atmospheric modelling of the background contribution upon space measurements of ground reflectance, including bi-directional properties, *Appl. Opt.* 18:3587–3594.

Tanré, D., Deroo, C., Duhaut, P., Herman, M., Morcrette, J. J., Perbos, J., and Deschamps, P. Y. (1985), Effets atmosphériques en télédétection, logiciel de simulation du signal satellitaire dans le spectre solaire, in *Proc. 3rd Int. Coll. on Spectral Signatures of Objects in Remote Sensing*, Les Arcs, France, 16–20 Dec., ESA SP-247, pp. 315–319.

Tanré, D., Deschamps, P. Y., Duhaut, P., and Herman, M. (1987), Adjacency effect produced by the atmospheric scattering in Thematic Mapper data, *J. Geophys. Res.* 92:12000–12006.

Verdin, J. P., Eckhardt, D. W., and Lyford, G. R. (1987), Evaluation of SPOT imagery for monitoring irrigated lands, in *Proc. Int. Conference on SPOT 1, Image Utilization, Assessment, Results*, Paris, 23–27 Nov. 1987, Cepadues, Paris, pp. 81–90.

Welch, R., and Ehlers, M. (1986), Merging multiresolution SPOT HRV and Landsat TM data, *Photogramm. Eng. Remote Sens.* 53(3):301–303.

Welch, R., Jordan, T. R., and Ehlers, M. (1985), Comparative evaluation of the geodetic accuracy and cartographic potential of Landsat-4 and Landsat-5 Thematic Mapper image data, *Photogramm. Eng. Remote Sens.* 51(9):1249–1262.